CHALMERS
UNIVERSITY OF TECHNOLOGY

Chemical vapor deposition of TiN on transition metal substrates

Surface & Coatings Technology 334 (2018) 373–383

Contents lists available at ScienceDirect

Surface & Coatings Technology

journal homepage: www.elsevier.com/locate/surfcoat

Chemical vapor deposition of TiN on transition metal substrates

L. von Fieandt[a,*], T. Larsson[b], E. Lindahl[c], O. Bäcke[d], M. Boman[a]

[a] Uppsala University, Department of Chemistry, Ångström Laboratory, Lägerhyddsvägen 1, Box 538 75120, Uppsala, Sweden
[b] Seco Tools AB, Björnbacksvägen 2, 73782 Fagersta, Sweden
[c] AB Sandvik Coromant, Lerkrogsvägen 19, 12679 Hägersten, Sweden
[d] Chalmers University of Technology, Department of Applied Physics, 41296 Göteborg, Sweden

ARTICLE INFO

Keywords:
CVD
TiN
Alternate binder phase
Thermodynamic calculations

ABSTRACT

The growth of chemical vapor deposited TiN from a reaction gas mixture of $TiCl_4$, N_2 and H_2 was investigated on three different transition metal substrates: Fe, Co and Ni at deposition temperatures ranging from 850 °C to 950 °C. The interactions between the substrate metals and the gas phase were investigated using thermodynamic calculations. The TiN coatings were characterized by scanning electron microscopy, scanning transmission electron microscopy, X-ray diffraction, energy dispersive X-ray spectroscopy and transmission Kikuchi diffraction.

Chemical vapor deposition (CVD) of TiN on Co substrates resulted in dense, columnar coatings of single phase TiN. The activation energy for TiN deposition on Co was determined to be 90 kJ/mol. CVD of TiN on Fe substrates caused severe substrate corrosion by the formation of gaseous $FeCl_x$. Due to the substrate corrosion, the activation energy could not be determined. Furthermore, it was found that CVD of TiN on Ni substrates produced a phase mixture of TiN and Ni_3Ti. Formation of Ni_3Ti could be minimized by decreasing the H_2 partial pressure and increasing the N_2 partial pressure. Deposition on Ni yielded two different activation energies, 40 kJ/mol in the temperature interval 850 °C to 900 °C and 165 kJ/mol in the interval 900 °C to 950 °C. This is an indication of two different types of process control, which were identified as Ni diffusion into the growing film and a gas phase processes. The results of the present study showed that CVD of TiN on a cemented carbide using Fe and Ni in the binder phase, must be optimized in order to avoid corrosion or unwanted phases. Methods to achieve this are presented in this paper.

1. Introduction

Cemented carbide (WC with Co as a binder phase) based cutting tools have, for decades, been the primary choice in the metal forming industry. Lately, concerns regarding the toxicity of cobalt powder have increased, thereby driving the development for alternative binder phase materials [1,2]. Fe and Ni have been evaluated as such an alternative, showing promising results [3]. At the same time, the demands for higher quality and productivity are steadily increasing and the need to develop high performance tools is greater than ever. To increase the wear resistance of a cutting tool, hard protective coatings are typically applied by either chemical vapor deposition (CVD) or physical vapor deposition (PVD), depending on the intended use of the tool. CVD coated WC-Co cutting tools are often coated with a multilayer system comprising TiN-Ti(C,N)-Al_2O_3, where TiN is the layer closest to the tool material. A general prerequisite for CVD is that the substrate needs to be relatively inert towards the reaction gas-mixture in order to prevent substrate degradation (often by corrosion). If the binder phase of the WC-Co is changed, the interactions between the gas phase and the new binder needs to be investigated in order to maintain a high performance of the coating/substrate.

CVD of TiN on cemented carbides (WC/Co) is a well-known process [4–9]. Investigations of TiN deposition onto several binder phase candidates such as Ni and stainless steel have been performed, where a different growth rate, texture and coating morphology was observed on CVD of TiN [10,11]. The adhesion of the TiN coating was also lowered. As shown in previous studies the diffusion of binder phase material into the coating can also have a substantial impact on the coating adhesion [8,12,13]. In a study of CVD coating adhesion on WC substrates using different binder phases (Fe, Ni and Co based) it was found that Co containing substrates had the best tool–coating adhesion [3].

Porous coatings generally have poor mechanical properties, such as hardness and adhesion, and are thus not ideal for metal cutting applications. CVD growth of TiN on Ni surfaces have shown that the coating becomes porous and consists of more than one phase [11,13,14]. The cause of this behavior is suspected to arise from the interaction between

* Corresponding author.
E-mail address: linus.fieandt@kemi.uu.se (L. von Fieandt).

https://doi.org/10.1016/j.surfcoat.2017.11.063
Received 28 July 2017; Received in revised form 23 November 2017; Accepted 24 November 2017
Available online 26 November 2017

$TiCl_4$ and Ni to form Ni-chlorides in the gas phase. These compounds are reduced and redeposited on the TiN surface to form the inter-metallic compound Ni_3Ti. The reported growth of TiN on Ni substrates suggests that the required mechanical properties for cutting tool use cannot be achieved. However, through a better understanding of the interface chemistry during CVD of TiN the formation of inter-metallic phases can be suppressed.

The suggested rate limiting step in CVD of TiN from the $TiCl_4$-N_2-H_2 system in conditions where mass transport influence is minimal, is breakage of H−H and N≡N bonds on the growing surface [15]. The required dissociation and recombination energies for both gases depends on the surface. Of importance for the surface reactions are the surface chemical composition, the surface structure and therefore the crystallographic orientation of the surface [16]. Another important reaction involved in the formation of TiN from the $TiCl_4$-N_2-H_2 reaction gas mixture is the homogeneous reduction of $TiCl_4$ to $TiCl_3$ and $TiCl_2$ in the gas phase where $TiCl_3$ is believed to be the main Ti growth species. The reduction reaction $TiCl_4 \rightarrow TiCl_{4-x}$ is favored in the presence of hydrogen through the formation of HCl instead of Cl_2 [17–19]. Furthermore, it was shown in [19] that $TiCl_{4-x}$ does not form in significant amounts in the absence of H_2 at temperatures ≤ 1000 °C. In the presence of H_2 the onset of $TiCl_{4-x}$ formation occurs at significantly lower temperatures, ~800 °C [19]. TiN is normally deposited in an excess of H_2, thus enabling fast reduction of $TiCl_4$ to $TiCl_{4-x}$. However, CVD in a H_2 deficient atmosphere may shift the $TiCl_4/TiCl_3$ equilibrium and reduce the reactivity of the Ti-precursor.

In this paper the growth mechanism of CVD of TiN on binder phase candidates Fe and Ni have been investigated. The insights in the growth mechanism will be used to propose a deposition method for TiN coatings suitable for cutting tool applications where Fe and/or Ni is used as binder. Thermodynamic calculations were performed to predict and interpret the experimental results. Co substrates were used as a reference in all experiments. Pure metallic substrates were implemented in this study, in order to clarify the effect of changing the binder, as in most previous cases alloys were studied and thus the effect of each metal is unclear.

2. Material and methods

An Ionbond 530 hot wall CVD reactor was used to deposit TiN layers on Co, Fe and Ni substrates. The overall chemical reaction for the TiN formation can be described as:

$$2\,TiCl_4(g) + N_2(g) + 4H_2(g) \rightarrow 2TiN(s) + 8HCl(g)$$

The deposition conditions are shown in Table 1. Five depositions were made with a step wise (25 °C) increase of temperature between 850 and 950 °C. One deposition was performed at 950 °C with a reduced H_2 partial pressure compared to the other depositions. The deposition time was adjusted to give the same film thickness for all depositions.

Table 1
Temperature, partial pressures for all gases and deposition time for the TiN depositions.

T (°C)	H_2 (kPa)	N_2 (kPa)	$TiCl_4$ (kPa)	P_{tot}(kPa)	Deposition time (h)
850	42.2	16.7	1.1	60	7.5
875	42.2	16.7	1.1	60	5.0
900	42.2	16.7	1.1	60	4.5
925	42.2	16.7	1.1	60	4.5
950	42.2	16.7	1.1	60	2.3
950 (reduced H_2)	7.6	51.3	1.1	60	2.3

The Fe substrates were produced by pressing and arc melting Fe powder (Alfa Aesar, 99.9%). The Fe substrates were ground flat using SiC paper and polished to a mirror finish using 6, 3 and 1 μm diamond suspensions as final polish. Polished metallic Co (99.5% and Ni(99.9%) substrates (10 × 10 × 1 mm) were supplied by MTI Corp.

The phase content of the TiN coatings were analyzed using grazing incidence X-ray diffraction (GI-XRD) at 1° incidence angle, using a Philips MRD-XPERT diffractometer. An incident beam X-ray mirror was used in all measurements. For the coatings deposited on Ni substrates, a 0.27° parallel plate collimator and a 0.04 rad Soller slit were used on the diffracted side. For the coatings deposited on Fe and Co substrates a 0.18° parallel plate collimator, flat graphite monochromator and 0.04 rad Soller slit were used on the diffracted side.

Polished cross sections of the deposited coatings were produced by cutting with an alumina high-speed cutter and casting into Bakelite. The cast samples were ground flat using SiC paper (120 − 1000) and then polished using a diamond slurry (6, 3 and 1 μm particle sizes) followed by a final polish using colloidal SiO_2.

A lamella from one of the Ni samples (deposition temperature 950 °C) for investigations by scanning transmission electron microscopy (STEM) and transmission Kikuchi diffraction (TKD) was produced using the Focused ion beam (FIB) in-situ lift out technique by an FEI Strata DB 235 instrument [20]. Film morphology, cross section thicknesses, elemental composition and local phase composition of the CVD coatings were measured using a Zeiss Merlin High-resolution scanning electron microscope (HR-SEM). Coating growth rates were calculated by dividing cross section thickness with deposition time. Elemental composition was measured using energy dispersive x-ray spectroscopy (EDS) with an X-Max 80 mm^2 silicon drift detector. Local phase composition was measured by TKD measurements using an Oxford Nordlys EBSD detector.

A probe corrected Titan Themis operating at 200 keV was used for the TEM measurements. STEM images were acquired using a high angle annular dark field detector (HAADF). STEM-EDS analysis was performed using a SuperX – EDS detector.

3. Thermodynamic calculations

To aid the interpretation of the experimental results thermodynamic calculations were performed. The same experimental parameters as in the depositions were applied. One set of calculations was made for each of the substrate metals, the substrate metal was kept in a large excess to reflect the experimental conditions. To get the highest possible accuracy of the calculations all possible condensed and gaseous reaction products were included. 43 reaction products for CVD on Co substrates, 44 reaction products for CVD on Ni substrates and 51 reaction products for CVD on Fe substrates were included. For a detailed list of all species, see Appendix A, Table A1. A free-energy minimization technique was used, (program Ekvicalc [21]) This method was implemented to predict the behavior of CVD processes in several studies, thereby confirming the validity of the method [15,22,23]

4. Results and discussion

4.1. Thermodynamic calculations

The yield of substrate chlorides in the gas phase as a function of

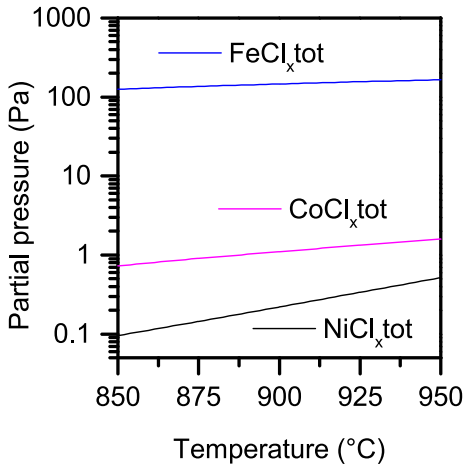

Fig. 1. Partial pressure of metal chlorides in the gas phase after TiN deposition. $FeCl_x$ tot = $FeCl_2$ + Fe_2Cl_4 + $FeCl_3$ + FeCl + Fe_2Cl_6. $CoCl_x$ tot = $CoCl_2$ + CoCl + Co_2Cl_4 + $CoCl_3$. $NiCl_x$ tot = NiCl + $NiCl_2$.

temperature is presented in Fig. 1.The yield of chlorides is an indication of how inert the substrate is towards the reaction gas mixture. The higher the yield of chlorides the more severe the corrosion of the substrate will be initially before an intact layer of TiN has formed on the substrate. Formation of $CoCl_x$(g) indicates that some etching of the Co substrate will take place. However, the calculated partial pressure of $CoCl_x$ is low and two orders of magnitude lower than that of $FeCl_x$. Thus, it can be concluded that the Co substrate will be less prone to etching than Fe. As can be seen, the $FeCl_x$(g) has the highest partial pressure of all the calculated substrate chlorides. The calculations indicate that the yield of Ni chlorides is even less than that of Co chlorides, see Fig. 1. The fact that the formation of gaseous Ni chlorides is so low suggests that the formation of a previously reported Ni_3Ti interphase is not caused by redeposition from the gas phase as suggested by Konyashin et.al [13]. In the calculations TiN was the only condensed phase forming.

4.2. Experimental results

The deposition time was varied in order to achieve coatings of equal thicknesses, the estimations were based on kinetic data from CVD of TiN on WC-Co substrates. The thicknesses for all deposited coatings are presented in Table 2. As can be expected, the thicknesses of the TiN films deposited on Co substrates were close to the expected thickness of 1 μm. However, the coatings deposited on Fe and Ni substrates deviated significantly. The nature of the deviations will be investigated and discussed in the following sections.

Table 2
Average coating thickness in μm for all deposition temperatures and substrates. *Coating thickness for Fe and Ni substrates are discussed in more detail in Sections 4.2.2 and 4.2.3 respectively.

Substrate	850 (°C)	875 (°C)	900 (°C)	925 (°C)	950 (°C)
Co	1.20	1.08	1.06	0.93	0.80
Fe*	0.65	0.71	0.45	0.20	0.18
Ni*	15.75	13.65	12.27	12.63	11.42

4.2.1. Co substrates

The TiN films grown on Co substrates have a morphology where ridge-like grains, needles and stars can be observed for all temperatures, see Fig. 2. A slight increase in the grain size for the layer deposited at 950 °C was observed, see Fig. 2e. The morphologies obtained on Co correspond with morphologies obtained on cemented carbides at similar temperatures [24]. The cross-section SEM image of the coating deposited at 875 °C shows a columnar and dense microstructure, see Fig. 2f. Cross sections at all other temperatures are shown in Appendix B, Fig. B1. The substrate/coating interface is sharp and without pores, indicating that the substrate is inert to the reaction gas mixture. This was also predicted by thermodynamic calculations.

The growth rate and calculated activation energy of the depositions on Co substrates is presented in Fig. 3a and b respectively. It was suggested in [25], that reactions controlled by surface kinetics have activation energies in the range 100–300 kJ/mol. In this investigation the calculated activation energy on Co was 90 kJ/mol which suggests that the deposition process is controlled by surface kinetics between 850 and 950 °C under the used conditions.

The GI-XRD diffractograms from CVD of TiN on Co substrates are shown in Fig. 4. Two phases are present: the Co substrate and the deposited TiN. No intermetallic crystalline phases between Co and Ti or $TiCl_x$ could be detected by GI-XRD. The peak positions of the TiN and the peak broadening are not affected by the temperature increase, implying constant compositions and similar grain sizes for all deposited coatings. The coating deposited at 950 °C was slightly thinner than the coatings at lower temperatures, 0.8 μm and ~1 μm respectively. The strong substrate peak observed in Fig. 4 is a result of the thinner coating at 950 °C.

4.2.2. Fe substrates

Fig. 5 shows the morphology and a cross section of the TiN coatings grown on Fe substrates. The grain morphology is a mixture of standing platelets, a small amount of star-shaped grains and areas of small needle-like grains. Smaller TiN grains were observed close to the substrate grain boundaries, see Fig. 5c, d and e. This indicates that there is a difference in deposition kinetics on Fe compared to TiN growth on Co substrates, where a completely different morphology was observed, see Fig. 2. The reason for this is that Fe is a very reactive substrate which can act as a reducing agent, forming $FeCl_x$(g). This will strongly influence the initial nucleation and growth of TiN.

The cross-section microstructure of the TiN layer deposited on Fe at 875 °C, depicted in the SEM image in Fig. 5f, shows rounded pits at the layer-substrate interface. Cross sections at all other deposition temperatures are shown in Appendix C, Fig. C1. Ferrous materials exposed to chlorides commonly show grain boundary corrosion [26]. The grain boundary corrosion is visualized in the top view micrographs in Fig. 5a–e, where the substrate grain boundaries are observed and the deposited TiN has a smaller grain size. Corrosion can also be seen in Fig. 5f, where pits are clearly visible at the substrate-coating interface. The corrosion of the substrate is most likely caused by formation of $FeCl_2$(g) as suggested by the thermodynamic calculations.

Growth rate measurements of TiN on Fe substrates was complicated since a homogeneous sharp interface could not be identified, see Fig. 5f.

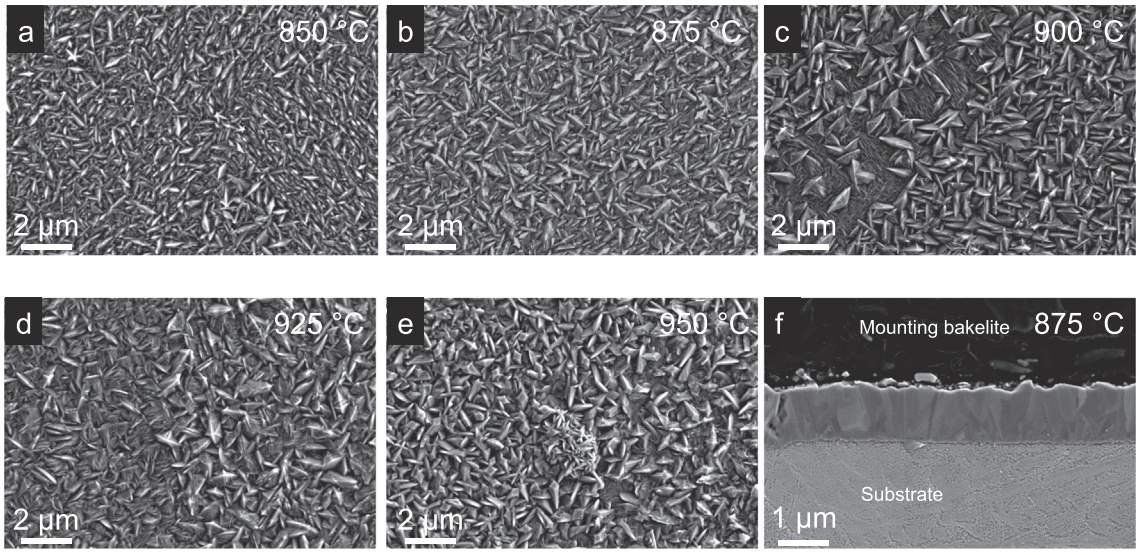

Fig. 2. SEM micrographs of the coatings deposited on Co substrates at 850–950 °C (a–e) respectively. A cross-section micrograph of the 875 °C deposition in f.

Etching of the substrate prior to formation of a fully covering TiN layer resulted in pits and porosity in the substrate, making total coating thickness measurements impossible.

The phase content of the coatings deposited on Fe substrates was investigated by GI-XRD. It was found that TiN successfully deposited on Fe substrates, as shown in Fig. 6. No traces of any crystalline etching products, such as iron chlorides were identified by GI-XRD. Furthermore, no traces of chlorides could be found when the coatings were analyzed by EDS (not shown here). The substrate peaks increased in intensity as the deposition temperature was increased. This is because the etching of the substrate is faster at higher temperatures and will yield a more porous surface. It follows that coatings deposited into the substrate pores will yield a layer that appears thinner in GI-XRD and so the substrate peaks will therefore be more intense.

4.2.3. Ni substrates

CVD of TiN on Ni substrates had a morphology that was different from the coatings deposited on both Fe and Co. The top-view SEM micrographs in Fig. 7a–d show nodular grains, a morphology not observed before. The cross-section micrograph in Fig. 7f from the

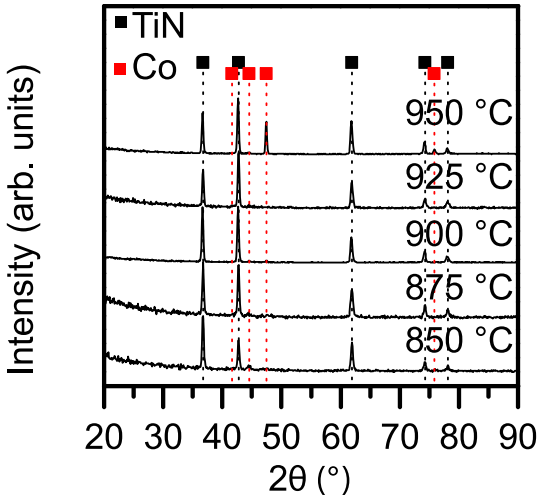

Fig. 4. GI-XRD diffractograms of the coatings deposited onto Co substrates.

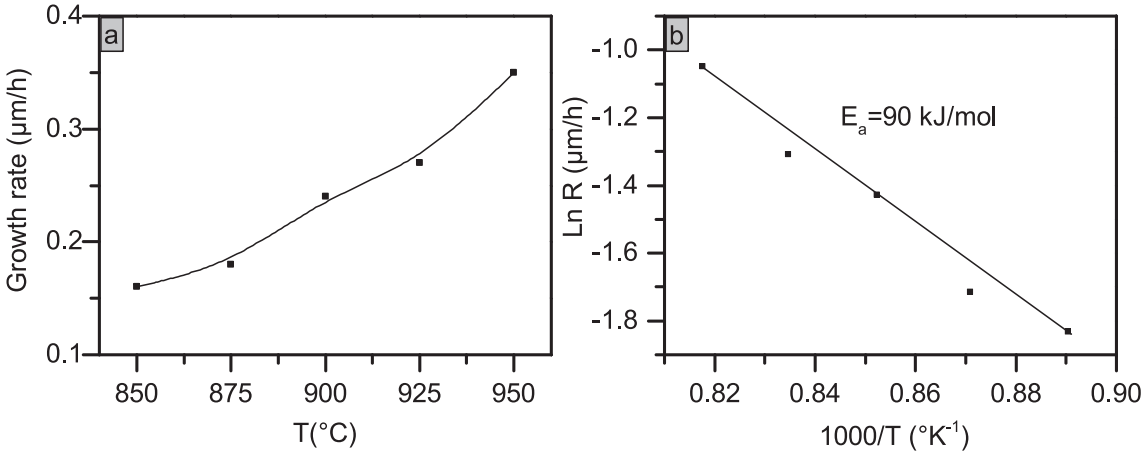

Fig. 3. a) Growth rate of TiN on Co substrates. The line is a guide for the eye b) Arrhenius curve, activation energy indicated in the figure.

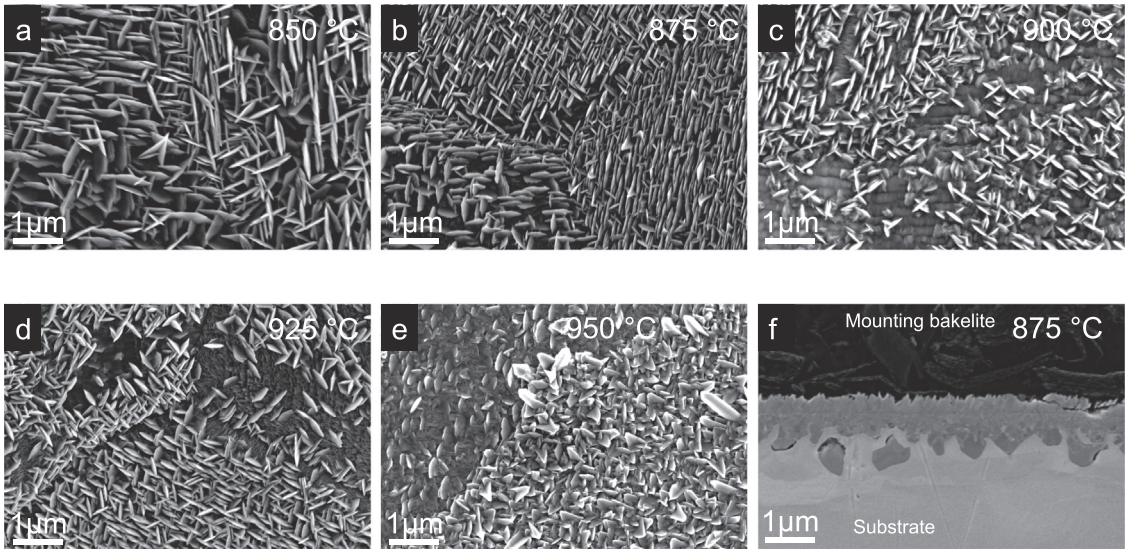

Fig. 5. SEM micrographs of the coatings deposited on Fe substrates at 850–950 °C (a–e) respectively. Cross-section micrograph of the 875 °C deposition in f.

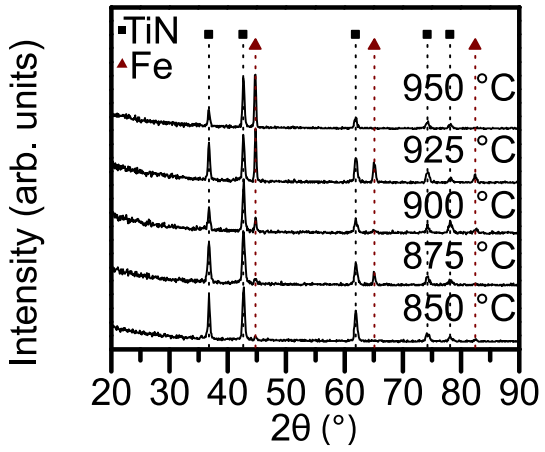

Fig. 6. GI-XRD diffractograms of the coatings deposited on Fe substrates.

deposition at 875 °C, which is representative for all coatings on Ni, shows a non-homogeneous microstructure with a porous region suspected to be the interface between the substrate (dashed line in Fig. 7f) and the coating.

As can be seen in Fig. 7f, CVD of TiN on Ni did not yield homogenous coatings. Rather deposits containing a mixture of two or more phases having a porous non-homogeneous microstructure with areas of brighter contrast covered by thin areas having a darker contrast were observed. Cross sections from the other deposition temperatures, can be found in Appendix D, Fig. D1. The growth rates, presented in Fig. 8a, were determined by measurements of the thickness of the mixed phase area. It is evident from the Arrhenius plot of the growth data, Fig. 8b, that there are two distinct linear regions with the inclination point at 900 °C. At temperatures below 900 °C the calculated activation energy is low (E_a = 40 kJ/mol) indicating a reaction limited by mass transport. The linear region at temperatures higher than 900 °C has a significantly higher activation energy (E_a = 165 kJ/mol) indicating a kinetically controlled process.

The phase composition determined by GI- XRD was Ni_3Ti and TiN, see Fig. 9. The presence of Ni_3Ti has been observed previously for CVD of TiN on Ni substrates even at lower temperatures (700 °C) than in this investigation. Although, it was reported to be pure TiN and $TiCl_2$, which appears to be a misinterpretation since no traces of $TiCl_2$ could be found in this study [11].

It is important to note that the growth rate in Fig. 8 represent growth of both TiN and Ni_3Ti. If Ni is involved by diffusion from the substrate the growth rate of the multi-phase film has a contribution from two different processes, solid state diffusion and gas phase reactions. The rate limiting process was determined by the Arrhenius dependences. Depending on the temperature this will be observed in the Arrhenius plot as two regions with different slopes as seen in Fig. 8b. However, the picture is complicated since the CVD reaction may be transport-limited at high temperatures.

In order to further investigate the phase content and microstructure, a TEM lamella was made from the coating deposited on Ni at 950 °C. The cross-section was analyzed using HAADF-STEM and EDS, see Fig. 10a–d. The brighter grains consist of a mixture of Ni and Ti as well as areas of only Ni. N is not present. The darker areas in Fig. 7f and Fig. 10a are composed of Ti and N, indicating the presence of TiN. The EDS analysis revealed no traces of Cl, thus indicating that no Cl containing compounds were present in the coating.

The lamella was further analyzed using TKD, Fig. 11a, where it was established that the darker areas are composed of TiN. Further, the TKD analysis revealed two additional phases, hexagonal Ni_3Ti and cubic Ni. The results are in agreement with the findings from the EDS analysis where the darker areas consisted of Ti and N and the brighter areas of either Ni and Ti or only Ni. The bright contrast at the coating/substrate interface shown in Fig. 7f, indicates that this area consists solely of Ni_3Ti and metallic Ni. Thus, no TiN formed directly on the substrate. The metallic Ni found at the top of the coating by TKD and TEM,

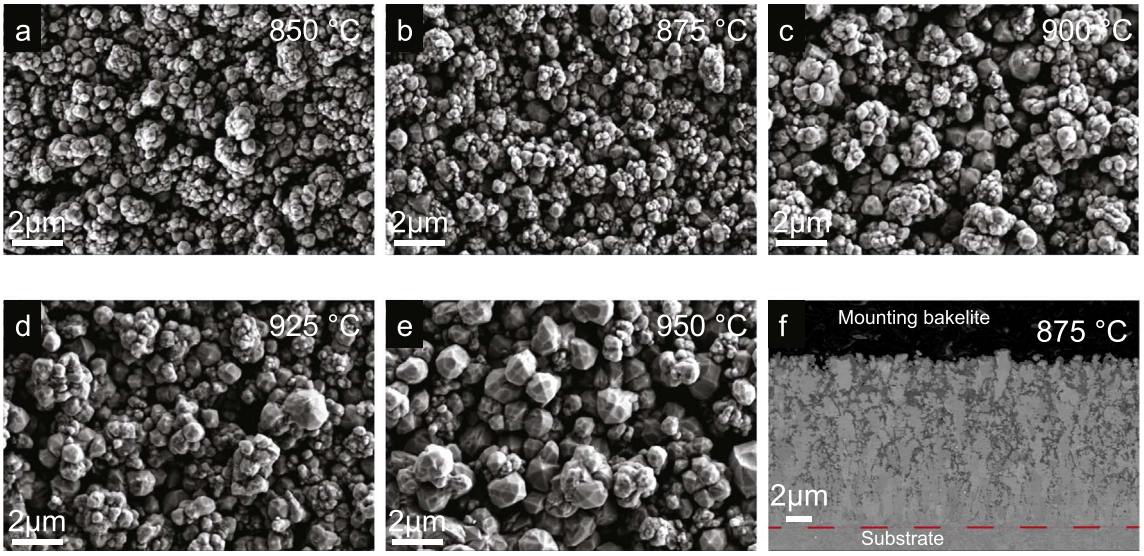

Fig. 7. SEM micrographs of the coatings deposited on Ni substrates at 850–950 °C (a-e) respectively. Cross-section micrograph of the 875 °C deposition in f, coating substrate interface indicated by the red line, below which only metallic Ni was detected. (For interpretation of the references to colour in this figure legend, the reader is referred to the web version of this article.)

Figs. 10 and 11, could be a result of Ni_3Ti decomposition with subsequent TiN formation through interactions with N_2 in the gas phase and Ti in Ni_3Ti. This suggests that a single-phase TiN coating is difficult to deposit under the conditions used here, at least until the surface is fully covered by Ni_3Ti.

Since no solid Ni_3Ti was expected to form based on the thermodynamic calculations, the observed formation of Ni_3Ti must be favored kinetically over TiN formation. It was suggested that the recombination rate of N_2 on a Ni surface is greater than the dissociation rate [16]. In such a case, the kinetic barrier of N_2 dissociation is even more pronounced on a Ni surface, compared to, for instance, Co. This assumption is supported by the experimental data where no TiN could be found in the substrate/coating interface, see Fig. 7f.

The pores found at the metal-deposit interface in Fig. 7f are likely to be caused by rapid diffusion. Since Ni is found at the surface of the coating it means that Ni must have diffused from the substrate to the top of the coating, a distance of about 12 μm in about 2.3 h. If it is assumed that Ni is diffusing in either a Ti or Ni matrix the diffusion rate is in agreement with tabulated values [27]. Considering also that no TiN is formed on top of the Ni substrate, it can be assumed that limited or negligible diffusion occurs in TiN. Furthermore, the obtained microstructure is porous, which results in even higher diffusion rates by grain boundary diffusion. The rate of diffusion can be lowered by a reduced reaction temperature, thus minimizing the formation of Ni_3Ti. However, a reduced reaction temperature would require a change of N-precursor from N_2 to a more reactive molecule, e.g. NH_3 [28–31].

We suggest that the Ni_3Ti phase is formed due to a low activity of N_2 on the Ni surface and a high activity of $TiCl_{4-x}$ on the same surface. This

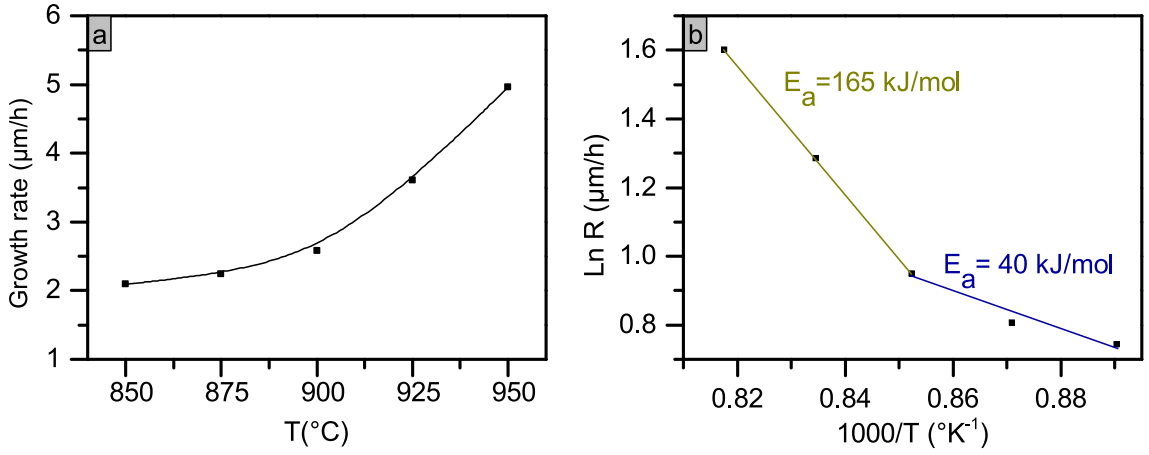

Fig. 8. a) Growth rate of TiN and Ni_3Ti on Ni substrates b) Arrhenius curve, two different activation energies indicated by the two dashed lines.

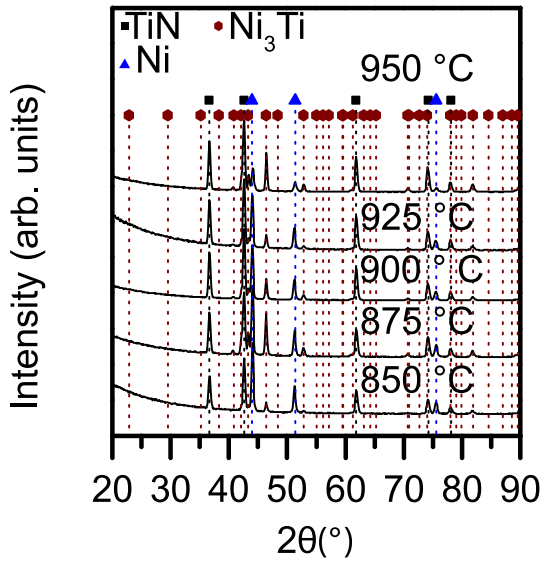

Fig. 9. GI-XRD diffractograms of the coatings deposited on Ni substrates.

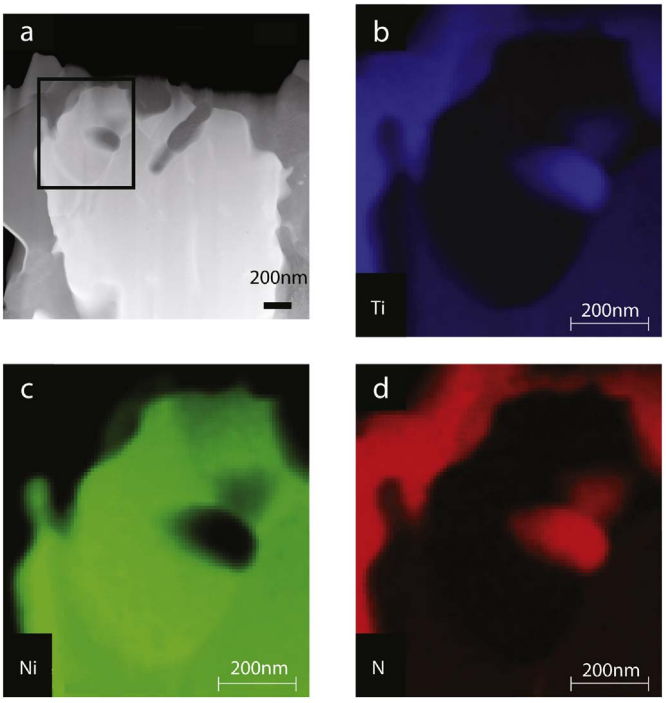

Fig. 10. a) STEM-HAADF micrograph of the lamella from the Ni sample, depicting the top of the deposited layer, area EDS analysis, area marked with a black rectangle. b–d) EDS maps of Ni, Ti and N respectively.

leads to the conclusion that there are two possible ways to minimize the formation rate of Ni_3Ti: either by reducing the H_2 partial pressure, or by increasing the N_2 partial pressure. A reduced H_2 partial pressure would lower the reduction rate of $TiCl_4$ and an increased N_2 partial pressure would increase the probability of surface reaction between dissociated N species and Ti.

4.2.4. Deposition with reduced H_2 partial pressure and increased N_2 partial pressure

TiN was also deposited in an experiment with a reduced H_2 partial pressure/increased N_2 partial pressure on a Ni substrate to investigate the hypothesis in section 4.41. Deposition with reduced H_2 partial pressure resulted in a coating with multimodal grain morphology, see Fig. 12a. Comparing grain morphologies of depositions using high and low H_2 partial pressures, Figs. 7a–e and 12, shows clear differences. Deposition with reduced H_2 shows both standing platelets (as for Fe substrates), ridges (as for Co substrates), as well as star-shaped grains and agglomerates of small needle-shaped grains. The agglomerates are observed on what is believed to be the substrate grain boundaries, indicating a different growth mechanism or growth of a different phase at the grain boundaries. The cross-section micrographs in Fig. 12b and c shows a reduced amount of mixed phase areas compared to the depositions at higher partial pressure of H_2, see Fig. 7f. The area indicated in Fig. 12c was further examined by an EDS line scan, see Fig. 12d. The coating contains mostly Ti and N in the darker areas and mostly Ni in the brighter areas. The presence of Ni_3Ti, Ni and TiN in the coating deposited with reduced H_2 partial pressure was confirmed by GI-XRD, see Fig. 13.

The lower H_2 partial pressure resulted in lowered Ni_3Ti formation. This shows that a reduction of the $TiCl_x$ sub chlorides, induced by the low H_2 partial pressure, minimizes the Ni_3Ti formation. This indicates that the reduction of $TiCl_4$ is most likely the rate determining step in the formation of Ni_3Ti from $TiCl_4$ and Ni. Furthermore, the increased N_2 partial pressure most likely increases the probability of surface reactions between Ti species and N_2. Thus, a reduced H_2 partial pressure and an increased N_2 partial pressure will reduce the formation rate of Ni_3Ti. In conclusion, a reduced $TiCl_4$ sub-chloride partial pressure and the increased probability of surface reactions between Ti species and N_2 increase the rate of TiN formation on Ni substrates.

5. Conclusions

In the present work the phase content, growth rate, morphology and microstructure of CVD of TiN from $TiCl_4$, N_2 and H_2 was investigated on Fe, Ni and Co substrates. Fe and Ni are candidates to replace Co as a binder phase in cemented carbides.

Thermodynamic calculations predicted that Ni substrates would be the most stable substrate towards etching by the reaction gas phase followed by Co. Fe substrates were predicted to be etched by the reaction gas mixture through the formation of $FeCl_x(g)$.

Deposition on Co substrates resulted in dense columnar TiN coatings and no substrate corrosion was observed, irrespective of the deposition temperature.

Experimentally CVD of TiN on Fe substrates resulted in single-phased TiN coatings; however, the substrates were etched by the gas phase as predicted by thermodynamic calculations. A higher deposition temperature resulted in a higher degree of substrate etching. If iron will be used as a binder phase it is therefore recommended to keep the deposition temperature as low as possible, at least initially in the CVD process.

Deposition of TiN on Ni substrates proved to be complicated due to

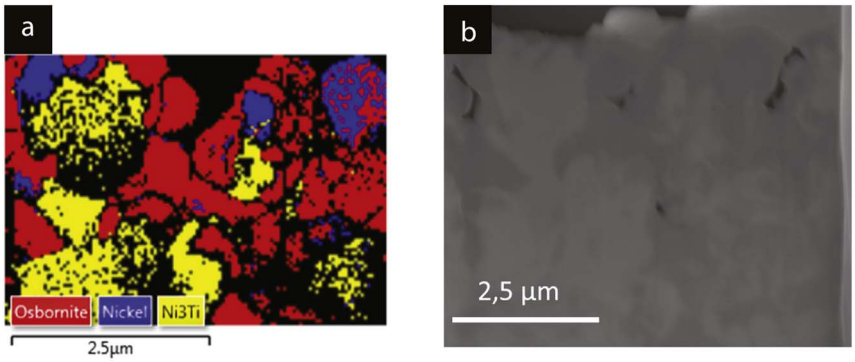

Fig. 11. a) TKD map of the top part of the deposit, red corresponds to Osbornite(TiN) blue corresponds to metallic Ni and, yellow corresponds to Ni_3Ti, black areas are areas with zero solutions b) SEM cross-section micrograph of area analyzed using TKD. (For interpretation of the references to colour in this figure legend, the reader is referred to the web version of this article.)

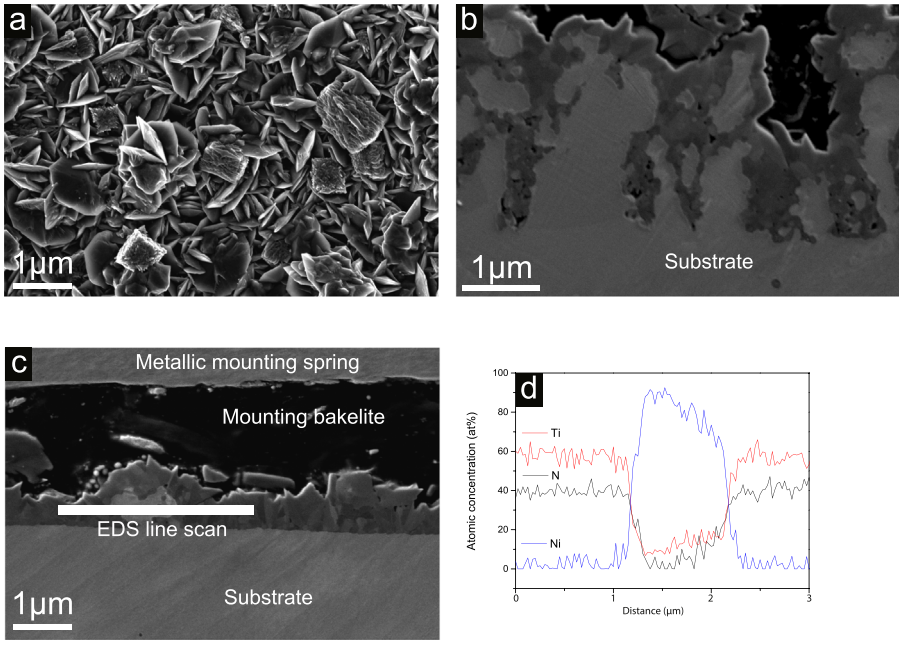

Fig. 12. a) Top view micrograph of the coating deposited on Ni using reduced H_2 partial pressure b) cross section overview of the multi-phase area, c) cross section micrograph of the same sample with area for EDS line scan indicated. d) EDS line scan of the area marked in (c).

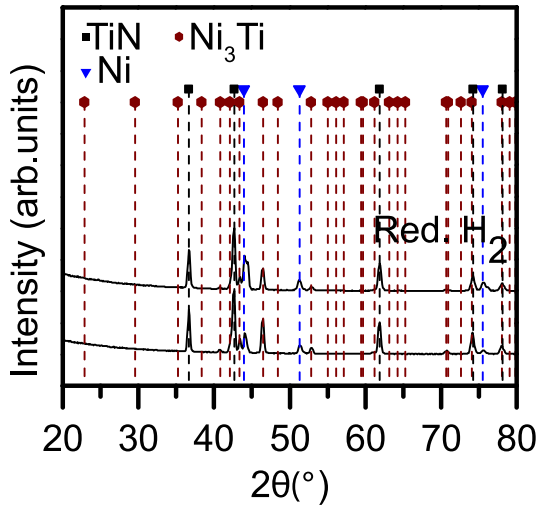

Fig. 13. GI-XRD diffractograms of the coating deposited on Ni substrates at 950 °C and the coating deposited at 950 °C with reduced H_2 partial pressure.

the formation of an intermetallic phase - Ni_3Ti. TiN was not observed at the substrate interface. Only when the Ni surface was completely covered by Ni_3Ti did TiN form. Furthermore, metallic Ni was observed at the top of the coating. This indicates problems during nucleation and initial growth resulting in poor quality coatings on Ni. The porous deposit formed on the Ni substrates is not favorable for cutting applications, as it will lead to poor coating-substrate adhesion. Furthermore, the mechanical properties of Ni_3Ti are not optimal for use in metal cutting and the formation of this phase is thus undesirable.

A hypothesis that formation of Ni_3Ti could be avoided through lowered H_2 partial pressures and increasing the N_2 partial pressure was tested. While the formation of Ni_3Ti was not completely inhibited, it was reduced significantly. This suggests that a large excess of N_2 and a low H_2 partial pressure is required to deposit TiN on a Ni based binder phase.

Acknowledgements

Funding of CVD 2.0 by the Swedish Foundation for Strategic Research via SSF contract RMA15-0048 is gratefully acknowledged. Funding from Sandvik AB is gratefully acknowledged.

Appendix A

Table A1

All substances used in the thermodynamic calculations with respective database reference.

Reference [32]	TiH2(s)	Reference [33]
H2(g)	N2H4(l)	Co(l)
N2(g)	Reference [34]	Co(alpha)
NH3(g)	HN3(g)	Co(beta)
H(g)	Reference [35]	Co(g)
NH2(g)	N3(g)	Co3N(s)
N(g)	HN(g)	Reference [36]
N2H2(g)	FeCl2(g)	Fe2N(s)
N2H4(g)	FeCl2(l)	TiCl4(g)
N3(g)	FeCl2(s)	TiCl4(s)
Cl(g)	Fe2Cl4(g)	TiCl4(l)
Cl2(g)	Reference [37]	FeTi(s)
HCl(g)	CoCl2(s)	Reference [38]
TiCl(g)	CoCl2(l)	TiN(s)
TiCl2(g)	CoCl2(g)	TiN(l)
TiCl3(g)	CoCl(g)	TiCl4(g)
TiCl3(s)	Co2Cl4(g)	TiCl4(s)
Ti(g)	CoCl3(g)	TiCl4(l)
FeCl3(g)	Reference [39]	NH4Cl(s)
FeCl3(s)	TiCl4(g)	N2H4(l)
FeCl3(l)	Ti2Cl6(g)	NiCl2(s)
FeCl(g)	Fe4N(s)	NiCl2(g)
Fe2Cl6(g)	Fe2N(s)	Reference [40]
Fe(g)	TiCl4(s)	Co(l)
Fe(l)	TiCl4(l)	Co(alpha)
Fe(gamma)	FeTi(s)	Co(beta)
Fe(alpha)	Ni(l)	Co(g)
Fe(delta)	Ni(alpha)	Co3N(s)
TiN(s)	Ni(beta)	
TiN(l)	NiTi(s)	
TiCl4(g)	NiTi2(s)	
TiCl4(s)	Ni3Ti(s)	
TiCl4(l)	NiCl(g)	
TiCl2(s)	Ni(g)	
Ti(beta)		
Ti(alpha)		
Ti(l)		

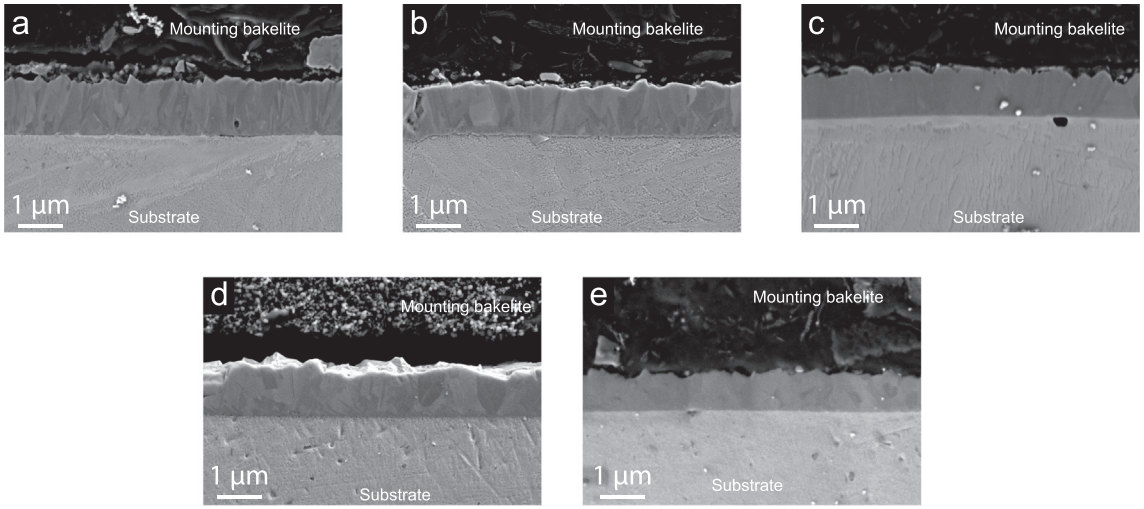

Fig. B1. SEM cross section micrographs of all coatings deposited on Co substrates 850–950 °C shown in a–e respectively.

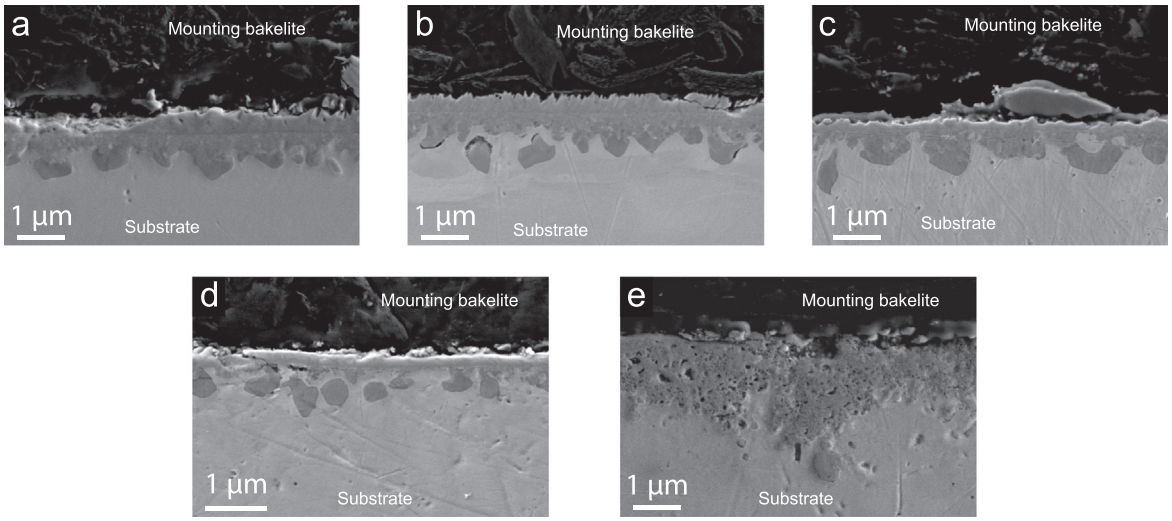

Fig. C1. SEM cross section micrographs of all coatings deposited on Fe substrates 850–950 °C shown in a–e respectively.

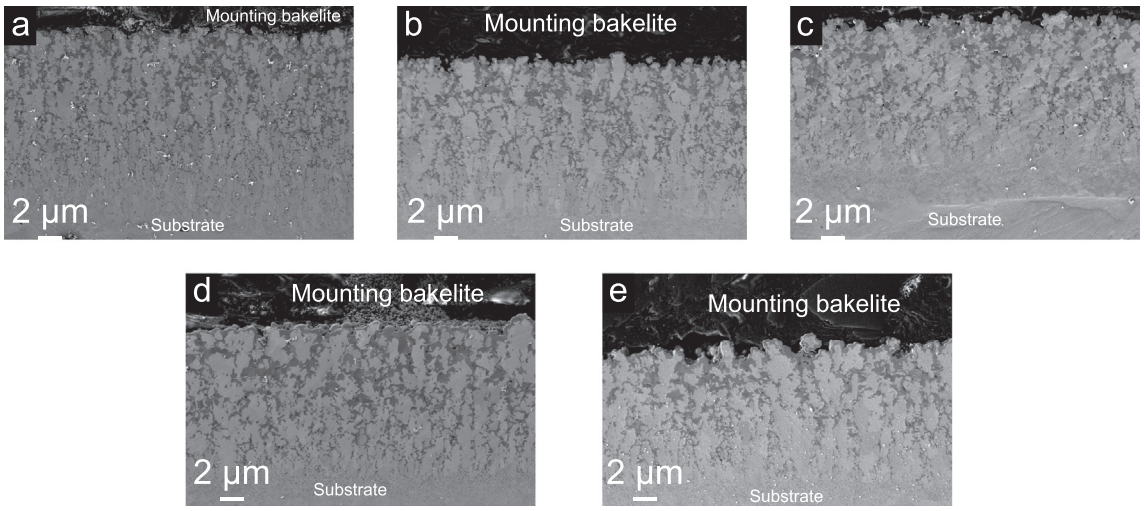

Fig. D1. SEM cross section micrographs of all coatings deposited on Ni substrates 850–950 °C shown in a–e respectively.

References

[1] S. Bastian, W. Busch, D. Kühnel, A. Springer, T. Meißner, R. Holke, et al., Toxicity of tungsten carbide and cobalt-doped tungsten carbide nanoparticles in mammalian cells in vitro, Environ. Health Perspect. 117 (2009) 530–535, http://dx.doi.org/10.1289/ehp.0800121.

[2] V. Richter, A. Potthoff, W. Pompe, M. Gelinsky, H. Ikonomidou, S. Bastian, et al., Evaluation of health risks of nano- and microparticles, Powder Metall. 51 (2008) 8–9, http://dx.doi.org/10.1179/174329008X286640.

[3] L. Toller, C. Liu, E. Holmström, T. Larsson, S. Norgren, Investigation of cemented carbides with alternative binders after CVD coating, Int. J. Refract. Met. Hard Mater. (2016), http://dx.doi.org/10.1016/j.ijrmhm.2016.07.005.

[4] J. Echigoya, Z. Liu, A. Imamura, S. Takatsu, Department of Materials Processing, Faculty of Eng&eering, 198 Tohoku University, Sendai 980 (Japan), 1991, pp. 293–300.

[5] A. Kafizas, C.J. Carmalt, I.P. Parkin, CVD and precursor chemistry of transition metal nitrides, Coord. Chem. Rev. 257 (2013) 2073–2119, http://dx.doi.org/10.1016/j.ccr.2012.12.004.

[6] H. Kashani, M. Heydarzadeh Sohi, H. Kaypour, Microstructural and physical properties of titanium nitride coatings produced by CVD process, Mater. Sci. Eng. A 286 (2000) 324–330, http://dx.doi.org/10.1016/S0921-5093(00)00744-9.

[7] H.E. Rebenne, D.G. Bhat, Review of CVD TiN coatings for wear-resistant applications: deposition processes, properties and performance, Surf. Coat. Technol. 63 (1994) 1–13, http://dx.doi.org/10.1016/S0257-8972(05)80002-7.

[8] W. Schintlmeister, Structure and strength effects in CVD titanium carbide and titanium nitride coatings, J. Electrochem. Soc. 123 (1976) 924, http://dx.doi.org/10.1149/1.2132969.

[9] J. Wagner, C. Mitterer, M. Penoy, C. Michotte, W. Wallgram, M. Kathrein, The effect of deposition temperature on microstructure and properties of thermal CVD TiN coatings, Int. J. Refract. Met. Hard Mater. 26 (2008) 120–126, http://dx.doi.org/10.1016/j.ijrmhm.2007.01.010.

[10] M.H. Staia, B. Lewis, J. Cawley, T. Hudson, Chemical vapour deposition of TiN on stainless steel, Surf. Coat. Technol. 76–77 (1995) 231–236, http://dx.doi.org/10.1016/0257-8972(95)02527-8.

[11] J.C. Nable, S. Nosheen, S.L. Suib, F.S. Galasso, Atmospheric pressure chemical vapor deposition of titanium nitride on metals, Surf. Coat. Technol. 200 (2006) 2821–2826, http://dx.doi.org/10.1016/j.surfcoat.2005.02.171.

[12] K. Akiyama, E. Nakamura, I. Suzuki, T. Oshika, A. Nishiyama, Y. Sawada, A study of the adhesion between CVD layers and a cemented carbide substrate by AEM analysis, Surf. Coat. Technol. 94–95 (1997) 328–332, http://dx.doi.org/10.1016/S0257-8972(97)00441-6.

[13] I.Y. Konyashin, Wear-resistant coatings for cermet cutting tools, Surf. Coat. Technol. 71 (1995) 284–291, http://dx.doi.org/10.1016/0257-8972(94)02326-L.

[14] W. Schintlmeister, Structure and strength effects in CVD titanium carbide and titanium nitride coatings, J. Electrochem. Soc. 123 (1976) 924, http://dx.doi.org/10.1149/1.2132969.

[15] N. Nakanishi, S. Mori, E. Kato, Kinetics of chemical vapor deposition of titanium nitride, J. Electrochem. Soc. 137 (1990) 322–328.

[16] H. Sellers, J. Anderson, Dissociation and recombination rate constants for N2 on Cu and Ni group transition metal surfaces, Surf. Sci. 475 (2001) 11–17, http://dx.doi.org/10.1016/S0039-6028(00)00969-9.

[17] J. Herzler, P. Roth, High-temperature decomposition of TiCl4 based on Cl-concentration measurements, Proc. Combust. Inst. 29 (2002) 1353–1359, http://dx.doi.org/10.1016/S1540-7489(02)80166-3.

[18] E.A. Haupfear, L.D. Schmidt, Kinetics and multiple steady states in the chemical vapor deposition of titanium carbide, J. Electrochem. Soc. 140 (1993) 1793–1801.

[19] F. Teyssandier, M.D. Allendorf, Thermodynamics and kinetics of gas-phase reactions in the Ti-cl-H system, J. Electrochem. Soc. 145 (1998) 2167–2178, http://dx.

doi.org/10.1149/1.1838613.
[20] R.M. Langford, C. Clinton, In situ lift-out using a FIB-SEM system, Micron 35 (2004) 607–611, http://dx.doi.org/10.1016/j.micron.2004.03.002.
[21] B. Noläng, Computer program Ekvicalc 4.6, Örnsätra, S-74386 Bälinge, Sweden, (1982).
[22] P. Stenberg, P. Sukkaew, I. Farkas, O. Kordina, E. Janzén, L. Ojamäe, et al., Silicon chemistry in fluorinated chemical vapor deposition of silicon carbide, J. Phys. Chem. C 121 (2017) 2711–2720, http://dx.doi.org/10.1021/acs.jpcc.6b10849.
[23] S. Leone, A. Henry, S. Andersson, O. Kordina, E. Janzén, Optimization of a concentrated chloride-based CVD process for 4H–SiC Epilayers, J. Electrochem. Soc. 157 (2010) H969–H976, http://dx.doi.org/10.1149/1.3473813.
[24] H.-E. Cheng, M.-H. Hon, Texture formation in titanium nitride films prepared by chemical vapor deposition, J. Appl. Phys. 79 (1996) 8047, http://dx.doi.org/10.1063/1.362358.
[25] J. Carlsson, Chemical Vapor Deposition, Handb. Depos. Technol. Film. Coatings, (2010), pp. 400–459, http://dx.doi.org/10.1016/B978-0-8155-2031-3.00007-7.
[26] C.X. Li, T. Bell, Corrosion Properties of Active Screen Plasma Nitrided 316 Austenitic Stainless Steel, 46 (2004), pp. 1527–1547, http://dx.doi.org/10.1016/j.corsci.2003.09.015.
[27] G. Neuman, C. Tuijn, Self-Diffusion and Impurity Diffusion in Pure Metals, vol. 14, Elsevier Ltd, 2008.
[28] S.R. Kurtz, R.G. Gordon, Chemical vapor deposition of titanium nitride at low temperatures, Thin Solid Films 140 (1986) 277–290, http://dx.doi.org/10.1016/0040-6090(86)90271-3.
[29] R.S. Larson, M.D. Allendorf, A reaction mechanism for titanium nitride CVD from TiCl4 and NH3, Proc. Thirteen. Int. Conf. Chem. Vap. Depos, 1996.
[30] H.H. Huang, M.H. Hon, M.C. Wang, Effect of NH 3 on the Growth Characterization of TiN Films at Low Temperature, 240 (2002), pp. 513–520.
[31] M. Grujicic, S.G. Lai, Multi-length scale modeling of chemical vapor deposition of titanium nitride coatings, J. Mater. Sci. 36 (2001) 2937–2953.
[32] D.R. Stull, H. Prophet, JANAF Thermochemical Tables, 2nd ed (NSRDS-NBS 37), 2nd ed., US Govt. Printing Office, Washington, 1971.
[33] I. Barin, O. Knacke, Thermochemical Properties of Inorganic Substances, Springer-Verlag, Berlin, New York, 1973.
[34] K.K. Kelley, High-temperature heat-content, heat-capacity, and entropy data for the elments and inorganic compounts, U.S Bur. Mines Bull, 584 1961, p. 592.
[35] M.W. Chase, J.L. Curnutt, A.T. Hu, A.N. Syverud, L.C. Walker, JANAF Thermochemical Tables, 1974 Supplement, (1974), http://dx.doi.org/10.1063/1.3253143.
[36] O. Kubaschewski, E.L. Evans, C.B. Alcock, Metallurgical Thermochemistry, 4th ed., Pergamon Press, Oxford, 1967.
[37] M.W. Chase, J.L. Curnutt, H. Prophet, R.A. Mcdonald, A.N. Syverud, JANAF Thermochemical Tables, 1975 Supplement JANAf Thermochemical Tables, 1975 Supplement, 1 (1996), http://dx.doi.org/10.1063/1.555517.
[38] O. Kubaschewski, C.B. Alcock, Metallurgical Thermochemistry, 5th ed., Pregamon Press, Oxford, 1979.
[39] I. Barin, O. Knacke, O. Kubaschewski, Thermochemical Properties of Inorganic Substances, Supplement, Springer, Berlin, 1977.
[40] R.R. Hultgren, Selected Values of Thermodynamic Properties of Metals and Alloys, Wiley, New york, 1963.